Percolation transitions in compressed SiO2 glasses

Anwar Hasmy
University Simon Bolivar
Simona Ispas
Montpellier University https://orcid.org/0000-0002-8537-8461
Bernard Hehlen (Bernard.hehlen@umontpellier.fr)
Montpellier University

Physical Sciences - Article

Keywords: SiO2 glasses, amorphous-amorphous transformations under, percolation transitions

Posted Date: April 19th, 2021

DOI: https://doi.org/10.21203/rs.3.rs-379312/v1

Version of Record: A version of this preprint was published at Nature on November 3rd, 2021. See the published version at https://doi.org/10.1038/s41586-021-03918-0.

Percolation transitions in compressed SiO_2 glasses

A. Hasmy[1,2], S. Ispas[1], and B. Hehlen[1]
[1] *Laboratoire Charles Coulomb (L2C), CNRS - Univ. Montpellier, 34095 Montpellier, France and*
[2] *Departamento de Física, Universidad Simón Bolívar, Valle de Sartenejas, Caracas, Venezuela*
(Dated: March 31, 2021)

Amorphous-amorphous transformations under pressure are generally explained by changes in the local structure from low to higher fold coordinated polyhedra [1–4]. However, as the notion of scale invariance at the critical thresholds has not been addressed, it is still unclear whether these transformations could be associated to true phase transitions. Here we report *ab initio* based calculations of compressed silica (SiO_2) glasses showing that the structural changes from low- to high-density amorphous structures occur through a sequence of percolation transitions. When the pressure is increased up to 82 GPa, a series of long range ('infinite') percolating clusters built up by corner- or edge-shared tetrahedra, pentahedra, and eventually octahedra, emerge at some critical pressures and replace the previous phase of lower fold coordinated polyhedra and lower connectivity. This mechanism provides a natural explanation for the well-known mechanical anomaly around 3 GPa as well as for the structural irreversibility beyond 10 GPa, among others. Some of the amorphous structures that have been discovered mimic those of coesite IV and V crystals reported recently [5, 6], highlighting the major role of SiO_5 pentahedra-based polyamorphs in the densification process of vitreous silica. Our observations demonstrate that the percolation theory provides a robust framework to understand the nature and the pathway of the amorphous-amorphous transformations, and open a new avenue to predict unraveled amorphous solid phases and related liquids [7, 8].

The understanding of the physical mechanisms controlling the transformation from one amorphous phase to another is an open fundamental issue in materials science [1, 2, 7, 9]. In amorphous solids such as SiO_2, GeO_2, Si, Ge and chalcogenides, short-range structures are very similar to those of the cristalline counterparts and it is the random nature of the inter-unit connections which makes the disorder at long length scale. In these systems, it has been argued that amorphous phases can be described in terms of changes of electronic and structural properties at short and medium range order. These properties are for example the electronic bonding [2, 4, 10, 11], the coordination number [1, 3, 4, 10, 12, 13] and the ring distribution [13, 14]. However, to describe the passage from one amorphous phase to another at the critical threshold, an explicit scale-invariant quantity (i.e. an order parameter) should be defined. This concept has yet never been considered for the pressure-driven amorphous solid transformations.

When an amorphous solid is pressurized, it is commonly assumed that the transformations from low to high density materials occur gradually, with coexisting low and high fold coordinated polyhedra. Such gradual change, sometime referred as *polyamorphism*, contrasts with the polymorphism in crystals, in which transitions occur from a specific phase to another at a critical pressure. In addition, it opposes to behaviors observed at rather well defined pressures. The change from tetrahedra (Z=4) to octahedra (stishovite-like structure, Z=6) structures in vitreous silica (v-SiO_2) is accompanied by the well known mechanical anomaly at 3 GPa [15, 16], a percolation phenomenon at $\simeq$ 8 GPa [17], and a two-steps elastic-to-plastic transformation, one around 10 GPa [14, 16, 18] and a second one around 20 GPa [16].

Ab initio methods have provided a key tool to clarify the pathway of the structural transformations in crystalline silicas (c-SiO_2) [5, 6, 19–21] and in amorphous materials. Recent artful machine learning *ab initio* method combined with empirical force field on compressed amorphous silicon highlights subsequent local changes that suggest a finite number of amorphous phases [4], but the description of the passage from one phase to another was not addressed. For v-SiO_2 at ambient pressure, *ab initio* methods have also nicely complemented experimental data [22, 23]. However, despite many efforts [14, 24, 25], its application to the above-mentioned issues has been limited due to the prohibitive calculation times required for a reliable thermodynamic sampling (in terms of system sizes, pressure steps as well time equilibration) [26, 27].

Herein lies our motivation to use an *ab initio* based approach, the Self-Consistent-Charge Density Functional based Tight-Binding (SCC-DFTB) method [28]. Combined with the Molecular Dynamics (MD) technique, it is able to reproduce many features of c-SiO_2 and v-SiO_2 with similar accuracy as *ab initio* methods, but being at least three order of magnitudes faster in terms of CPU time. This allowed us to simulate more than 40 SiO_2 glasses and to explore the full pressure range up to 82 GPa at room temperature. We also decompressed one of the resulting samples from 8 GPa and another from just above 10 GPa (for details see Methods). Our samples contain 1008 atoms (336 SiO_2 units) which is large enough to observe and describe the percolation critical phenomena governing the aforementioned transformations.

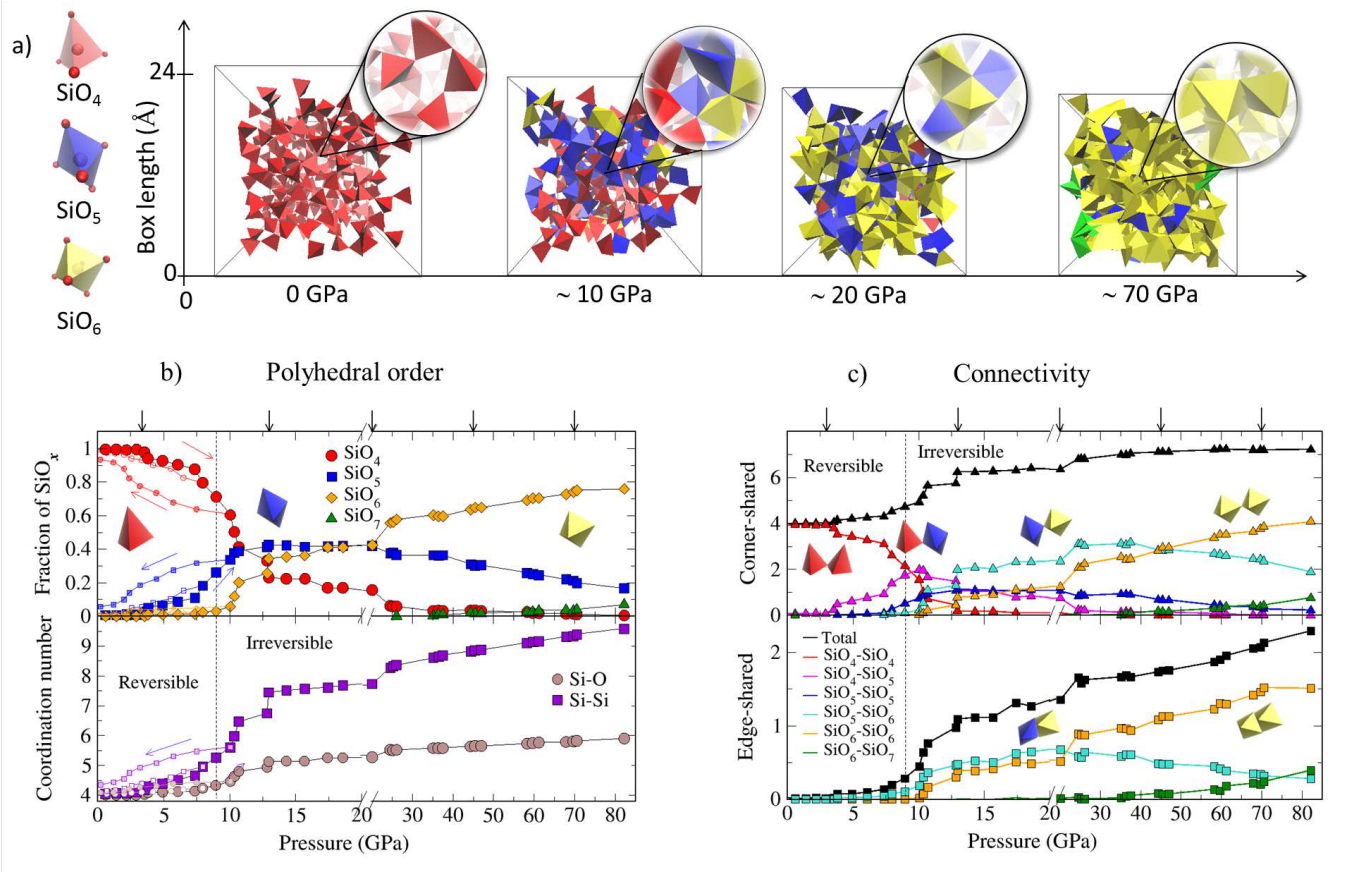

FIG. 1: (a) Snapshots of the simulation boxes showing the evolution of the short range structures from SiO_n to SiO_{n+1} polyhedra, and of their connectivity from corner- to edge-sharing connectivity (circular insets), upon pressure. The glass samples are pressurized by instantaneous reduction of the simulation box followed by a relaxation using periodic boundary conditions. (b) Fraction of Si polyhedra and Si-O and Si-Si coordination number as a function of pressure. Small symbols and arrows nearby correspond to unloadings from 8 GPa and slightly above 10 GPa. (c) Shared corners and shared edges per polyhedron. The bold vertical arrows on top in panels (b,c) mark the onset of the different regimes (see text) and the dashed line indicates the elastic to plastic transition. Note that the scale changes at 20 GPa in the abscissa axis.

Polyhedra coordination and connectivity.

Figure 1a illustrates the v-SiO_2 transformation from $Z = 4$ to 6 as the pressure P is increased. At ambient temperature and $0 < P < 3$ GPa, similarly to c-SiO_2, the Si-O bond of v-SiO_2 is characterized by a sp^3 hybridization which favors the formation of SiO_4 tetrahedra. However, for $3 < P < 10$ GPa, the densification of v-SiO_2 includes changes in the electronic structure, with an increase of the Fermi energy and of the atomic charges of O and Si (Extended Data Figs. 1 and 2). Theses changes produce an increase in the Si-O bonding ionicity (Extended Data Fig. 1c), boosting the formation of higher fold coordinated polyhedra (Fig. 1a,b). As a consequence, beyond 10 GPa the inter-polyhedra connectivity change from purely corner-sharing tetrahedra to a more complex connected network (Extended Data Figs. 3 and 4). The latter involves corner- and edge-sharing (Fig. 1a,c) SiO_5-SiO_6 and SiO_6-SiO_6 and to a lower extent face-sharing polyhedra (Extended Data Fig. 5).

We recall that on increasing the pressure from ambient conditions, c-SiO_2 passes from tetrahedral to octahedral ($Z = 6$) local structure through structural transformations including α-quartz to coesite I ($Z = 4$) at 3 GPa, then coesite I to stishovite (rutile structure, $Z = 6$) at 9 GPa. It is well known that the bonding is more ionic in the later that in the former case [11]. Regarding the connectivity of the polyhedra, since the oxygen atoms are divalent when $Z = 4$, each SiO_4 shares one oxygen atom (corner-sharing) with its four closest neighboring tetrahedra. This is the cases of v-SiO_2 and c-SiO_2 for $P < 3$ GPa and $P < 9$ GPa, respectively. In c-SiO_2, for $Z = 6$ and $P > 9$ GPa, the oxygen atoms are trivalent, hence each SiO_6 shares two couples of oxygen atoms with two different nearest neighboring octahedra (edge-sharing), while the other connectivities are corner-shared with the eight

octahedra nearest neighbors remaining. In v-SiO_2, the changes of polyhedra coordination and connectivity allow to identify different regimes (top arrows in Fig. 1b-c). For $13 < P < 20$ GPa, the compressed glasses contain almost similar fractions of SiO_4, SiO_5 and SiO_6, with a total number of shared edges per polyhedron $n_{es} \simeq 1.4$ and a small connectivity contribution of face-sharing polyhedra. This recalls the crystalline polymorph discovered recently, the so-called coesite IV [6], rarely observed for high-valence and low-coordinated cations in crystals, as it is at odds with the Pauling rule. For $20 < P < 45$ GPa, the fraction of SiO_6 octahedra increases with a jump, while the fraction of SiO_4 tetrahedra falls down to almost zero. Also, n_{es} increases to $\simeq 1.7$ and the presence of a small fraction of face-sharing polyhedra persists, which looks similar to coesite V, the second newly discovered c-SiO_2 polymorph [6]. For $45 < P < 70$ GPa, the network connectivity is fully dominated by SiO_6 octahedra, either corner-shared and edge-shared, and $n_{es} \simeq 2$, which suggests the emergence of a stishovite like phase. On increasing the pressure beyond 70 GPa, the total number of edge-sharing per polyhedra becomes greater than 2 due to the contribution of SiO_7 polyhedra, suggesting the emergence of a post-stishovite like phase [25, 29].

Finally, we calculated the fraction of Si polyhedra and the coordination number for unloadings from 8 GPa and slightly above 10 GPa. In the former case the decompression is reversible while not in the latter (small symbols in Fig. 1b). The pressure threshold at which irreversibility occurs nicely agrees with experimental observation [16]. When unloading from 10 GPa to ambient pressure, an hysteresis is clearly observed due to persisting residual SiO_5 pentahedra (hence $Z \neq 4$, Fig. 1b), confirming previous expectations and pointing out the key role of 5-fold coordinated polyhedra in the plastic-to-elastic transition of v-SiO_2 [14, 16, 18].

Percolation transitions. The above observations only include an evaluation of the local and medium range order. However, the nature of the phase transformations from one regime to another in compressed v-SiO_2 should also be substantiated by the structure at long length scale. This is the purpose of the forthcoming discussion. Indeed, we found that clusters built up of SiO_n polyhedra (including their mixtures SiO_n-SiO_m) eventually emerge and one of them becomes dominant and percolates, by spanning its structure from one side to the other side of the simulation box (Fig. 2a). This effect has important implications on the glass rigidity [17], and can be monitored by calculating the percolation probability, P_∞. The latter is frequently used as an order parameter for the analysis of a percolation phase transition. It tends to 1 (or 0) if the largest cluster percolates (or not) and the percolating cluster is representative of the new phase [30]. Accordingly, the notation $(SiO_n\text{-}SiO_m)_\infty$ used in the following corresponds to a percolating cluster built of an alternation of n- and m-fold coordinated polyhedra.

Figure 2b shows the percolation probability, P_∞, of the biggest cluster for connected networks of SiO_4, SiO_5 and SiO_6 polyhedra, and their mixtures, as a function of pressure in compressed v-SiO_2. For the $(SiO_4\text{-}SiO_4)_\infty$ cluster, P_∞ drops from 1 to 0 at 13 GPa. In addition, between 3 and 8 GPa, a new percolating cluster built up by a connected skeleton of alternating tetrahedra and pentahedra, $(SiO_4\text{-}SiO_5)_\infty$, emerges. This coincides with the percolation transition observed at 8 GPa [17]. With increasing pressure, two more percolating clusters appear at 10 GPa and coexist with the first one: one built up by connected SiO_5-SiO_5 pentahedra and the second by connected SiO_5-SiO_6 polyhedra. The percolating cluster structures containing a mixture of SiO_4 and SiO_5 between 8 and 10 GPa, as well SiO_6 between 10 and 13 GPa, recall the pressure-induced post-quartz amorphous phases reported previously [31, 32]. Then, at 13 GPa, a $(SiO_6\text{-}SiO_6)_\infty$ cluster appears and percolates. The coexistence of all these percolating clusters beyond 13 GPa is similar to the coesite IV, whose crystalline structure combines SiO_4-SiO_5, SiO_5-SiO_5, SiO_5-SiO_6 and SiO_6-SiO_6 planes in different crystallographic directions. By analogy, the coesite IV-like vitreous phase is labeled v-coesite IV in Fig. 2b.

Slightly above 20 GPa, SiO_4 tetrahedra vanish and accordingly, P_∞ of the $(SiO_4\text{-}SiO_5)_\infty$ cluster falls down to 0. Simultaneously, a percolating cluster $(SiO_6\text{-}SiO_{5,6})_\infty$ connected by edge-sharing SiO_5-SiO_6 and SiO_6-SiO_6 polyhedra emerges, together with some face-sharing contribution. In that pressure range, the amorphous phase (labeled v-coesite V in Fig. 2b) possesses the same dominant edge-sharing polyhedra connectivity as well as equivalent alternations of SiO_n-SiO_m polyhedra as in coesite V [6]. It also associates to the delayed revert structural transformation observed experimentally above $\simeq 20$ GPa in v-SiO_2 [16], suggesting that edge-shared structures remain stable during decompression.

The analyses of the percolation probability of a cluster built up of pure edge-shared octahedra, similar to the stishovite situation evidences that such cluster percolates around 40 GPa and, accordingly, a v-stishovite phase replaces the v-coesite V one (Fig. 2a-b). The pressure at which this occurs is in good agreement with the value reported for compressed v-SiO_2 when Z becomes equal to 6 [29]. Therefore, our results demonstrate that instead of a single and gradual transition, the mechanism of the structural transformation from Z=4 to 6 includes a series of percolation transitions between well defined amorphous phases (Fig. 2).

The correlation length ξ has been estimated in the pressure range where the different percolating clusters appear. This quantity accounts for the maximum length at which the scale invariance exists. At the thermodynamics limit, it is expected that such quantity diverges

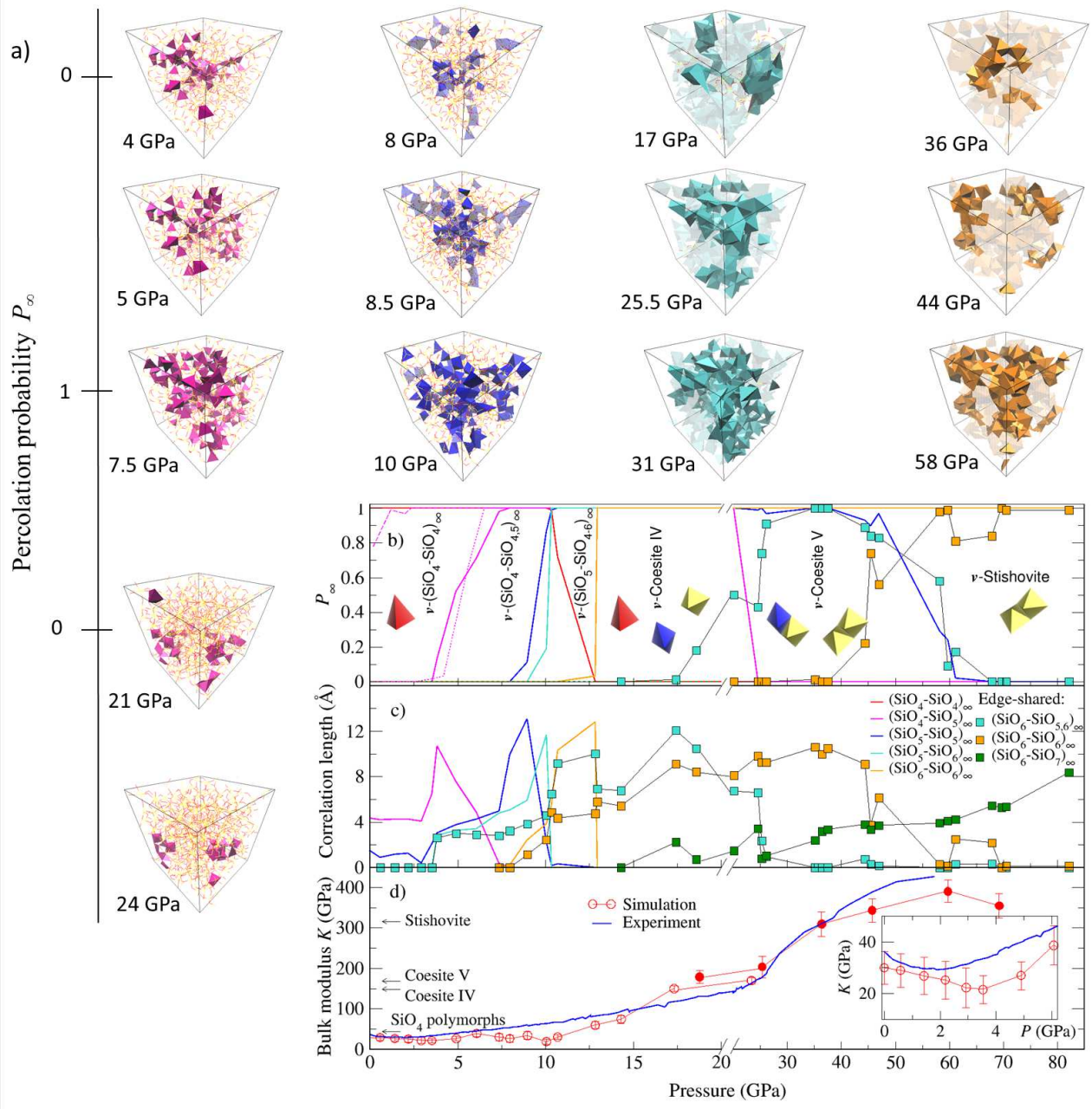

FIG. 2: (a) Snapshot of the spanning clusters in the simulation box for pressures corresponding to $P_\infty = 0$ up-to $P_\infty = 1$, and back to $P_\infty = 0$ for the first one. From left to right: corner-shared $(SiO_4\text{-}SiO_5)_\infty$ and $(SiO_5\text{-}SiO_5)_\infty$ clusters, and edge-shared $(SiO_6\text{-}SiO_{5,6})_\infty$ and $(SiO_6\text{-}SiO_6)_\infty$ clusters. (b) Percolation probability, P_∞, versus pressure for the different 4-, 5-, 6- and 7- folded coordinated Si, and their combinations. Dashed and dotted magenta lines correspond to P_∞ of the cluster $(SiO_4\text{-}SiO_5)_\infty$ for decompression from 8 GPa and 10 GPa, respectively. (c) Correlation length ξ of the percolating clusters in panel (b). (d) Bulk modulus K as function of pressure, and comparison with high frequency experiments (unrelaxed bulk modulus) [16]. The inset zooms on the low pressure region. Note that the scale changes at 20 GPa in the abscissa axis.

at the critical pressure, while it should reach a maximum for finite size systems as in our computer model. Indeed, for the different situations described above a maximum is always reached just before the corresponding critical pressure (Fig. 2c). Beyond 70 GPa a big cluster built up of edge-sharing $(SiO_6\text{-}SiO_7)_\infty$ polyhedra starts to grow, which, coupled to the fact that for such pressure the total number of shared edges per Si polyhedron exceeds 2, supports the post-stishovite like phase suggested above. The jump in the percolation probability P_∞ from 0 to 1

evidences the dominant character of a well-defined amorphous phase in a given pressure range. However, the non-negligible partial overlap between the ξ-curves beyond 13 GPa may indicates a phase coexistence between the dominant percolating cluster and the emerging one (Fig. 2c). This suggests that this phase acquires a metastable character when approaching the incoming critical pressure. Such behavior recalls the metastability observed in coesite IV and V crystalline polymorphs [5, 6].

When unloading from 8 GPa, the percolating $(SiO_4\text{-}SiO_5)_\infty$ cluster vanishes at a similar pressure at which it percolates during compression (Fig. 2b). This confirms the reversible character already suggested by the local and medium range structural analysis above. Conversely, when the sample is decompressed from 10 GPa (dashed curve), P_∞ exhibits a hysteresis, *i.e.* the $(SiO_4\text{-}SiO_5)_\infty$ cluster continues to percolate at pressures much lower than for the percolating compression route (Fig. 2b). A similar plastic behavior is observed for the other percolating clusters, *i.e.* $(SiO_5\text{-}SiO_5)_\infty$ and $(SiO_5\text{-}SiO_6)_\infty$ ones (data not shown). This shows that the formation of percolating clusters containing SiO_5 pentahedra for $P \gtrsim 10$ GPa prevents recovering the pristine glass structure, and likely explains the irreversible behavior.

To explore the impact of these percolation transitions on the glass rigidity, we calculated the bulk modulus K of our pressurized silicas (Fig 2d). As expected, the increasing connectivity at short and long length scales yields to a strong increase of K, i.e. from about 30 GPa at ambient conditions up-to $\simeq$ 375 GPa at $P = 82$ GPa. Its evolution nicely parallels that of the crystalline counterparts: SiO_4-polymorphs (except coesite I) below 10 GPa, coesite IV ad V at intermediate pressures, and stishovite above 35-40 GPa [6, 33]. Our calculations also reproduce the well know minimum around 3 GPa (inset of Fig. 2d). Following the percolation mechanisms discussed above, we associate the increased rigidity starting above 4 GPa to the series of the percolating clusters emerging upon pressure. Finally, our estimation of K is very close to high frequency experimental data except maybe around 10 GPa where the simulations exhibit a minimum, when $(SiO_5\text{-}SiO_5)_\infty$ and $(SiO_5\text{-}SiO_6)_\infty$ clusters emerge.

Additionally, for the different connectivity situations, we have analyzed the structure of the percolating cluster at the critical pressure thresholds. For this, we spanned these clusters taking into account the periodic boundary conditions before extracting them out of the box. Then, the structure of the isolated percolating clusters was analyzed by computing the structure factor $S(q)$. As expected from the percolation theory, at the critical thresholds, the cluster structures have fractal shapes, i.e. $S(q) \propto q^{-D_f}$ at intermediate wave-vector q-values, with $D_f \simeq 2.5$, which is also in agreement with the theoretical predicted value (Fig. 3).

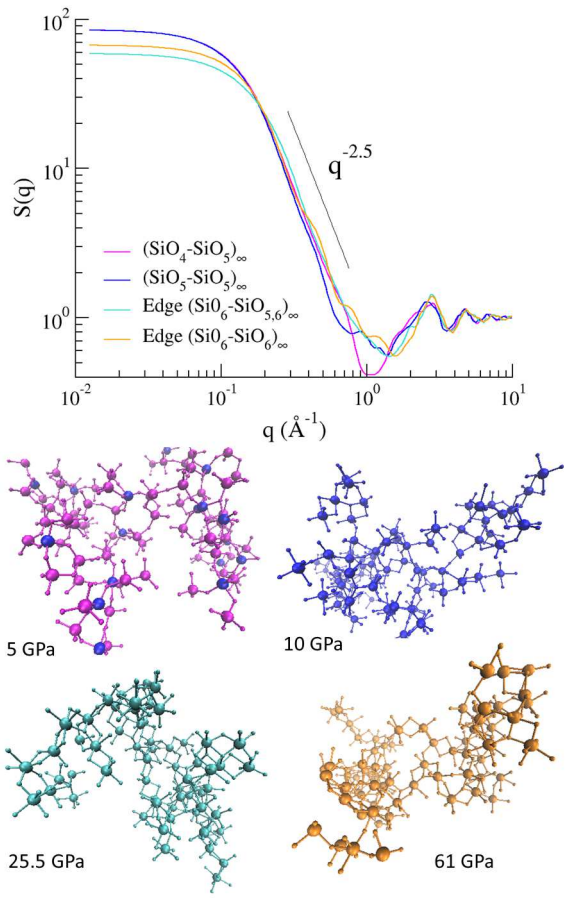

FIG. 3: Structure factors $S(q)$ for the isolated and extended percolating clusters at the critical pressures (indicated in the snapshots) in log-log scale.

CONCLUSIONS AND OUTLOOK

Our results show that in compressed v-SiO_2 the criticality of the amorphous-amorphous transformations can be described within the percolation theory by considering the percolation probability P_∞ as the order parameter. The long-range percolating clusters built up of different polyhedra coordination $(SiO_n\text{-}SiO_m)_\infty$ and connectivity (corner- or edge-shared) have the expected scale invariance at the critical threshold. The structure of these clusters beyond 13 GPa are similar to those of coesite IV, V and stishovite. The bulk moduli of the glass samples and the corresponding polymorphs are also similar. This suggests that the mechanical properties relate primarily to the peculiar connectivity describing the system at all length scales, rather than by the crystalline or amorphous nature of the network.

Our analysis is based on two central ideas that deserve to be considered in many other pressure- or temperature-driven amorphous-amorphous transformations, including oxide glasses, chalcogenides, metallic glasses, as well

as H_2O. The first one refers to the formation of long-range percolating clusters with a specific local coordination at a critical thermodynamical variable. Indeed, the temperature-driven amorphous transformations in liquid H_2O from the high to low density has been explained in these terms. The same has been argued for the glass transition in model systems [35–37] and seems also compatible with recent experimental observations [38]. The second one states that with pressure or temperature, the local coordination of materials built of polyhedra can evolve successively from low to high coordination through a series of percolation transitions. By providing an unified structural picture from short to long length scales of amorphous phases, these concepts could help to unveil affinities with crystalline polymorphs as well as to predict new phases appearing under extreme conditions.

METHODS

Glass preparation

The initial glass configuration containing 1008 atoms (336 SiO_2 units) placed in a cubic simulation box was prepared by carrying out classical MD simulations, using periodic boundary conditions. We used the melt-and-quench approach, the constant volume–constant temperature (NVT) ensemble and the atomic interactions were modelled using the BKS pair potential [39]. Then, we carried out MD simulations within the framework of the Self-Consistent Charge Density Functional based Tight-Binding (SCC-DFTB) method for the electronic structure calculations [28]. These calculations were also done using the NVT ensemble. The Andersen thermostat was used in order to maintain the room temperature and the samples were relaxed for more than 40 ps, with a time step equal to 2 fs. Within the SCC-DFTB approximation, the electronic integrals corresponding to the Hamiltonian matrix elements are replaced by analytical functions. The coefficients of these functions are obtained by fitting Density Functional Theory (DFT) calculations corresponding to systems obtained at different physico-chemical conditions. We used the PBC-0-3 set of parameters for SiO_2 [40]. This results in an electronic structure calculation method at least three orders of magnitude faster than DFT, currently considered the most performing *ab initio* method in materials science. The orbitals were occupied according to a Fermi–Dirac distribution with a temperature of 300 K. We included the Broyden charge mixing in the SCC cycle with a mixing parameter of 0.1. The Γ-point approximation was used for the electronic band structure energy and the projected electronic Density of States DOS calculations. For the latter, a gaussian broadening of 0.4 eV was considered.

Glass compression

The glass sample at ambient pressure prepared using the above procedure had a density of 2.3 g/cm^3. In order to mimic a quasi-statically compression, the box length was reduced by step of 1% (and atoms positions rescaled) after each 40 ps, until reaching a pressure of $\approx$ 27 GPa. A second series of glasses was obtained by instantaneous volume reduction of the sample obtained at 15 GPa yielding thereby seven samples at target pressures up to 82 GPa. Two successive volume reductions of 0.125% followed by a 40 ps relaxation were performed to 6 samples from this second series. The largest compression rate used here is almost equivalent to 0.02 GPa/ps. This corresponds to a compression velocity at least one order of magnitude slower than the one used in a previous DFT study of compressed SiO_2 at T=300 K [14], while the number of atoms in our calculation box is almost 7 times larger. In order to distinguish between the elastic and plastic regime, we also decompressed the samples from 8 and 10 GPa. This was done by increasing the box length and scaling the atom positions by 1% after each 40 ps, until reaching the ambient pressure. The reported structural quantities were averaged over all configurations generated in the last 10 ps of the sample relaxation time.

Electronic structure

For the simulated compressed glasses, we have analyzed the total and projected DOS, the Fermi energies and the Mulliken atomic charges $Q_{\rm Si}$ for Si and $Q_{\rm O}$ for O, as well the average Mulliken ionicity $\kappa_{\rm Si-O}$ calculated as done elsewhere [41]. For the latter, the relation $\kappa_{\rm Si-O} = |Q_{\rm Si}/\nu_{\rm Si} - Q_{\rm O}/\nu_{\rm O}|/2$ is used, where $\nu_{\rm Si}$ and $\nu_{\rm O}$ are the valence of Si and O atoms, respectively. The total and the projected O-2p DOS of the simulated glass at ambient pressure are in good agreement with experimental and DFT data [23] (Extended Data Fig. 1a). The effect induced by the sample densification in the total DOS of v-SiO_2 also agrees [11, 24] (Extended Data Fig. 1c,d). Similarly, the Si and O Mulliken atomic charges and the Si-O bond ionicity change is consistent with previous experimental and DFT findings [11, 14] (Extended Data Fig. 2). This favors the formation of pentahedra and higher fold coordinated Si polyhedra [42] (Fig. 1). The maxima reached in the pressure range 10-20 GPa where the SiO_5 fraction is dominant (Fig. 1), and the slight decreases beyond 20 GPa, highlight the large Si-O bonding ionic character of SiO_5 pentahedra compared to octahedra and tetrahedra.

Structure factor

In order to compare the structural properties of our samples to experimental data, we computed the neutron and X-ray total static structure factors. We firstly computed the partial structure factors $S_{\alpha\beta}(q)$ using the definition [43]:

$$S_{\alpha\beta}(q) = \frac{f_{\alpha\beta}}{N}\sum_{j=1}^{N_\alpha}\sum_{k=1}^{N_\beta}\langle\exp(i\vec{q}\cdot(\vec{r}_j-\vec{r}_k))\rangle \quad \alpha,\,\beta = \mathrm{Si,O}.$$

Here $f_{\alpha\beta} = 1$ for $\alpha = \beta$ and $f_{\alpha\beta} = 1/2$ otherwise, N_α is the number of particles of species α and N is the total number of atoms. The total structure factors are combinations of partial structure factors. For the neutron structure factor, we used the relation [43].

$$S_{\rm N}(q) = \frac{N}{\sum_{\alpha=\mathrm{Si,O}} N_\alpha b_\alpha^2}\sum_{\alpha,\beta=\mathrm{Si,O}} b_\alpha b_\beta S_{\alpha\beta}(q),$$

with the neutron scattering length b_α given by $b_{\rm Si} = 4.1491$ fm and $b_{\rm O} = 5.803$ fm, respectively [44]. The X-ray total structure factor $S_X(q)$ is given by [45]:

$$S_{\rm X}(q) = \frac{N}{\sum_\alpha N_\alpha f_\alpha^2(q/4\pi)}\sum_{\alpha,\beta} f_\alpha(q/4\pi) f_\beta(q/4\pi) S_{\alpha\beta}(q)\,.$$

Here $f_\alpha(s)$ is the scattering-factor function (also called form factor), computed as a linear combination of five Gaussians using the parameters derived elsewhere [46].

The calculated X-Ray $S_{\rm X}(q)$ and neutron $S_{\rm N}(q)$ structure factors are compared to experimental data [3, 13]. The calculated $S_X(q)$ reproduces the decrease and shift of the first sharp diffraction peak (FSDP) due to the collapse of the open structure of vSiO$_2$ at intermediate length scales (Extended Data Fig. 3).

Local connectivity

We computed the pair distribution function (PDF) $g_{\alpha\beta}(r)$ for all compressed v-SiO$_2$ samples using the definition [43]:

$$g_{\alpha\beta}(r) = \frac{V}{N_\alpha(N_\beta - \delta_{\alpha\beta})} \left\langle \sum_{i=1}^{N_\alpha} \sum_{j=1}^{N_\beta} \frac{1}{4\pi r^2} \delta(r - |\vec{r}_i - \vec{r}_j|) \right\rangle ,$$

where $\langle\cdot\rangle$ represents the thermal average, V is the volume of the simulation box, and $\delta_{\alpha\beta}$ is the Kronecker delta. For each of the three pairs, the first peak of the corresponding PDF corresponds to the distribution of the first neighbors shell distances Si-O, O-O and Si-Si, respectively. For the Si-O pair, a minimum after the first peak located at 2.3 Å defines rather well the upper limit of this distribution at all pressures. We used this value as a cutoff distance to estimate the Si-O coordination number and the fraction of SiO$_n$ polyhedra for the considered pressures. Similarly, a cutoff of 3.5 Å was used to identify the first Si-Si neighbors and to estimate the evolution of the polyhedra coordination number with pressure (Fig. 1b). The identification of the Si-O and Si-Si first neighbors also allowed to estimate the number oxygen atoms shared by two Si polyhedra neighbors, i.e, one, two, three or more, corresponding to corner-, edge- and face-shared polyhedral connectivity, respectively (Fig. 1c and Extended Data Fig. 5). The computed SiO distances are compared with experimental data in Extended Data Fig. 4a. The agreement is remarkable in particular in view of recent X-Ray measurements [3]. O-O and Si-Si distances are also shown for information.

The Si-O-Si and O-Si-O bond-angle distributions (BAD) and their pressure dependence are plotted in Extended Data Fig. 4b-c. The above mentioned up-shift of the FSDP translates into a fast reduction of the angles up to the first plastic transformation around 10 GPa when corner shared SiO$_5$- and SiO$_6$-based percolating clusters emerge. With increasing pressure above 10 GPa, and in addition to the primary peak at $\approx 130^o$, we notice the occurrence of two other peaks pointing at $\approx 98^o$ and $\approx 68^o$, respectively, in the bond angle distribution of Si-O-Si. The position of the three peaks shows a weak pressure dependence, while the two peaks located at smaller angles become prominent in the pressure range of v-Coesite IV and V for the first one, and v-Stishovite for the second. The Si-O and Si-Si bond lengths exhibit anomalies at pressures $\sim$ 10 GPa and 20-25 GPa corresponding to the two stages of plastic transformation, and the O-O bond length presents a maximum at pressure around 3 GPa corresponding to the minimum of the bulk modulus.

In order to give more insights in the medium range of the silica network with increasing pressure, we computed the ring distributions. No changes occurs for pressures below 4 GPa. Then, for pressures below 8 GPa, we observed a mild increase of the small ring sizes (2-, 3- and 4-membered ones) accompanying by the decrease of the proportion of large ring sizes (7- and 8-membered ones). When approaching the threshold the plastic regime at $\approx$ 10 GPa, the same pressure dependences were observed but presenting stronger trends. This increase of small rings at the expense of large ones at high pressure confirms previous DFT calculations [14].

Cluster analysis

To identify the different clusters with a specified polyhedra coordination and connectivity, as well the biggest one, we use a strategy inspired by the Friends-of-Friends algorithm which is widely used to characterize dark matter halos from N-body simulations [47]. In our implementation the first nearest neighbors correspond to the specific Si-O coordination and polyhedra connectivity we want to analyze. To determine if the biggest cluster percolates or not, we first extract all clusters from the box excepting the biggest one. Then we replicate the box containing this cluster along the three spatial directions. The Friends-of-Friends algorithm is applied again, and if the resulting biggest cluster is larger than the box size in at least two directions, we assume that the cluster percolates. For a given pressure, the above procedure is implemented to each SiO$_n$-SiO$_{n+1}$ possible connectivities, that is corner-, edge-, and face-shared polyhedra.

The percolation probability P_∞ is defined as the number of times the resulting biggest cluster percolates during the last 10 ps of the relaxation time, normalized by the total number of explored configurations. The correlation length ξ was calculated using the definition [30]:

$$\xi^2 = \frac{\sum_s 2R_{g,s}^2 s^2 n_s}{\sum_s s^2 n_s},$$

where $R_{g,s}$ and n_s are the gyration radius and the number of clusters of size s, respectively. The sum runs over all clusters of size s, excluding the biggest one if it percolates. The gyration radius $R_{g,s}$ was estimated using the relation:

$$R_{g,s}^2 = \frac{1}{2s^2} \sum_{i,j} r_{ij}^2,$$

where the sums run over pairs of Si atoms belonging to each cluster of size s. The correlation length ξ is averaged over the last 10 ps of the relaxation time.

Mechanical properties

We estimated the bulk modulus K of the compressed glasses by using the relation $K = -VdP/dV$, where V is the sample volume and P is the pressure averaged over the last 10 ps of the relaxation time. To obtain K we used the central difference scheme, and its

error bar is calculated by error propagation while the pressure error was estimated from the standard deviation. To minimize errors on the finite difference, when two subsequent pressures lie within the estimated error bars, the second is excluded from the estimation of K. We recall that volumetric measurements give direct access to the static compressibility [15], while high frequency experiments measure the volumetric variations at the time scale of the relaxational processes probed by the instrument [16]. In compressed v-SiO_2, both values are similar in the elastic regime ($P < 10$ GPa), but strong variations have been observed in the plastic case for $10 < P < 55$ GPa [16, 48, 49]. Intriguingly, above 12 GPa, our K calculated values are much closer to the high frequency data than to the static ones, a behavior which possibly reflects the typical time relaxation ($\simeq 10$ ps, corresponding to GHz frequencies) and the small volumetric variation (<0.4 nm^3) we used for the estimation of K in our MD simulations. For $P > 55$ GPa, the experimental value (static and high frequency) is $\simeq 420$ GPa [48, 49] in good agreement with our calculations.

Affinities with c-SiO_2 polymorphs

To identify the SiO_2 polymorph most akin to amorphous phases, we built supercells containing 582 atoms for tridymite, cristobalites, coesites and stishovite, and 432 and 486 atoms for β- and α-quartz, respectively. The unit cells of the polymorphs were obtained from the crystallographic databases [50]. These supercells are relaxed using the L-BFGS minimization method implemented in the DFTB+ package. Only the lengths of the lattice vectors were allowed to vary during the structure optimization, with the exception of coesite IV and V to preserve the same sample densities reported in Ref. [6].

The criterion used to define the v-coesite IV phase relies on the coexistence of $(SiO_4\text{-}SiO_5)_\infty$, $(SiO_5\text{-}SiO_5)_\infty$, $(SiO_5\text{-}SiO_6)_\infty$ and $(SiO_6\text{-}SiO_6)_\infty$, percolating clusters. We found that almost all SiO_5-SiO_6, SiO_6-SiO_6 are edge-shared, with a weak contribution of face-sharing polyhedra as in coesite IV and V. Indeed, in coesite IV we have validated the coexistence of different crystalline planes having the above-mentioned connectivities.

Edge-sharing SiO_5-SiO_6 and SiO_6-SiO_6 polyhedra become preponderant at $P \simeq 20$ GPa. They are in similar proportion, $\simeq 40$ %, and control the network connectivity as in coesite V. Beyond 40 GPa the fraction of SiO_5 starts to fall and the SiO_6-SiO_6 connectivity becomes dominant, which allows to identify the stishovite-like phase.

In order to validate the observations above, the total DOS, Fermi energy, Mulliken atomic charges and bond ionicity were computed and compared to the results obtained for compressed v-SiO_2 (Extended Data Figs. 1-2). The electronic properties of v-SiO_2 appear to be closer to α-quartz than to other SiO_4-based polymorphs at ambient pressure as suggested elsewhere [11]. On increasing pressure, the electronic properties of the vitreous polyamorphs, v-coesite IV, v-coesite V, and v-stishovite, are also compatible with those of coesite IV, V and stishovite crystals, respectively. The ionic character of the Si-O bond is also larger for the 5- and 6-fold Si coordinated polyhedra [20]. Similar conclusion holds when comparing the polyhedra coordination and connectivity with the corresponding v-SiO_2 percolating clusters, as well as for the calculated bulk moduli. The latter agrees very well with that of SiO_4-tetrahedra-based polymorphs at low pressures and to that of coesite IV, V, and stishovite (Fig. 2c) when pressure increases beyond 13 GPa.

Finally, Extended Data Table 1 gives the densities of the crystalline polymorphs and indicate the corresponding pressure ranges [6, 31, 51, 52]. The comparison with the corresponding polyamorph phases of v-SiO_2 is striking. One notices, for example, that a small pressure of $\simeq 3$ GPa is enough to compact the open structure of vitreous silica up to a density very close to that of α-quartz. At high pressure, the density-ranges of the polyamorphs follow that of the crystalline counterparts.

Percolating clusters at the critical threshold

We analyzed the structure of the percolating clusters around the critical pressures. For this we expanded and extracted out of the box the percolating clusters by taking into account the periodic boundary conditions. At the critical threshold, these clusters are usually larger than the box size due to their branched structure. We computed the structure factor $S(q)$ of the isolated clusters by using the corresponding expression for a diluted system [53]:

$$S(q) = 1 + \frac{1}{N}\sum_{i\neq j}\frac{\sin(qr_{ij})}{qr_{ij}},$$

where N is the number of Si atoms and q is the modulus of the wave vector. This expression implies that $S(0) = N_{Si}$ and $S(\infty) = 1$, where N_Si is the number of polyhedra (Si atoms). Besides, for fractal structures, at intermediate q values, $S(q)$ scales as q^{-D_f}, where D_f is the fractal dimension (Fig. 3).

[1] McMillan, P.F., Wilson, M., Daisenberger, D. & Machon, D. A density-driven phase transition between semiconducting and metallic polyamorphs of silicon. *Nat. Mater.* **4**, 680 (2005).

[2] Sheng, H.W. *et al.*. Polyamorphism in a metallic glass. *Nat. Mater.* **6**, 192 (2007).

[3] Prescher, C. *et al.* Beyond 6-fold coordinated Si in SiO_2 glass at ultrahigh pressures. *Proc. Natl. Acad. Sci. U.S.A.* **114**, 10041-10046 (2017).

[4] Deringer, V.L. *et al.* Origins of structural and electronic transitions in disordered silicon. *Nature* **589**, 59 (2021).

[5] Hu, Q.Y. *et al.* Polymorphic phase transition mechanism of compressed coesite. *Nat. Commun.* **6**, 6630 (2015).

[6] Bykova, E. *et al.* Metastable silica high pressure polymorphs as structural proxies of deep Earth silicate melts. *Nat. Commun.* **9**, 4789 (2018).

[7] Loerting, T., Brazhkin, V.V. & Morishita, T. Multiple amorphous-amorphous transitions. *Adv. Chem. Phys.* **143**, 29-82 (2009).

[8] Debenedetti, P.G. & Stillinger, F.H. Supercooled liquids and the glass transition. *Nature* **410**, 259-267 (2001).

[9] Brazhkin, V.V., Lyapin, A.G. & Trachenko, K. Atomistic modeling of multiple amorphous-amorphous transitions in SiO2 and GeO2 glasses at megabar pressures. *Phys. Rev. B* **83**, 132103 (2011).

[10] Principi, E. *et al.* Polyamorphic transition of germanium under pressure. *Phys. Rev. B* **69**, 201201(R) (2004).

[11] Lin, J.-F. *et al.* Electronic bonding transition in compressed SiO_2 glass. *Phys. Rev. B* **75**, 012201 (2007).

[12] Lelong, G. *et al.* Evidence of fivefold-coordinated Ge atoms in amorphous GeO_2 under pressure using inelastic x-ray scattering. *Phys. Rev. B* **85**, 134202 (2012).

[13] Zeidler, A. *et al.* High pressure transformation of SiO_2 glass from a tetrahedral to an octahedral network: a join approach using neutron diffraction and molecular dynamics. *Phys. Rev. Lett.* **113**, 135501 (2014).

[14] Ryuo, E., Wakabayashi, D., Koura, A. & Shimojo, F. *Ab initio* simulation of permanent densification in silica glass. *Phys Rev. B* **96**, 054206 (2017).

[15] Tsiok, O.B., Brazhkin, V.V., Lyapin, A.G. & Khvostantsev, L.G. Logarithmic kinetics of the amorphous-amorphous transformations in SiO_2 and GeO_2 glasses under high pressure. *Phys. Rev. Lett.* **80**, 999-1002 (1998).

[16] Weigel, C. *et al.* Pressure-induced densification of vitreous silica: Insight from elastic properties. *Phys. Rev. B* **100**, 094102 (2019).

[17] Trachenko, K., Dove, M.T., Brazhkin, V. & El'kin, F.S. Network rigidity and properties of SiO_2 and GeO_2 glasses under pressure. *Phys. Rev. Lett.* **93**, 135502 (2004).

[18] Liang, Y., Miranda, C.R. & Scandolo, S. Mechanical strength and coordination defects in compressed silica glass: Molecular dynamics simulations. *Phys. Rev. B* **75**, 024205 (2007).

[19] Martonák, R., Donadio, D., Oganov, A.R. & Parrinello, M. Crystal structure transformations in SiO_2 from classical and *ab initio* metadynamics *Nat. Mater.* **5**, 622-626 (2006).

[20] Yi, Y.S. & Lee, K.L. Pressure-induced changes in local electronic structures of SiO 2 and MgSiO 3 polymorphs: Insights from ab initio calculations of O K-edge energy-loss near-edge structure spectroscopy. *Amer. Mineral.* **97**, 897–909 (2012).

[21] Lyle, M.J., Pickard, C.J. & Needs, R.J. Prediction of 10-fold coordinated TiO_2 and SiO_2 structures at multimegabar pressures. *Proc. Natl. Acad. Sci. U.S.A* **112**, 6898-6901 (2015).

[22] Sarnthein, J., Pasquarello, A. & Car, R. Origin of the high-frequency doublet in the vibrational spectrum of vitreous SiO_2. *Science* **275**, 1925-1927 (1997).

[23] Hosokawa, S. *et al.*. Oxygen 2*p* Partial Density of States and bond angles around O atoms in SiO_2 glass. *J. of Phys. Soc. Jap.* **84**, 024605 (2015).

[24] Wu, M., Liang, Y., Jiang, J.-Z & Tse, J.S. Structure and properties of dense silica glass. *Sci. Reports* **2**, 398 (2012).

[25] Murakami, M. *et al.* Ultrahigh-pressure form of SiO_2 glass with dense pyrite-type crystalline homology. *Phys. Rev. B* **99**, 045153 (2019).

[26] Harvey, J.P. & Asimow, P.D. Current limitations of molecular dynamic simulations as probes of thermophysical behavior of silicate melts. *Amer. Mineral.* **100**, 1866–1882 (2015).

[27] Kob, W. & Ispas, S. First-principles simulations of glass-formers. *Encyclopedia of Glass Science, Technology, History, and Culture* Wiley Hoboken, NJ, ed. P. Richet (2020) arXiv:1604.07959

[28] Aradi, B., Hourahine, B. & Frauenheim, T. DFTB+, a sparse matrix-based implementation of the DFTB method. *J. Phys. Chem. A* **111**, 5678-5684 (2007).

[29] Sato, T. & Funamori, N. High pressure structural transformation of SiO_2 glass up to 100 GPa. *Phys. Rev. B* **82**, 184102 (2010).

[30] Sauffer, D. & Aharony, A. *Introduction to percolation theory* (Taylor & Francis, 2003).

[31] Hu, Q.Y. e*et al.* Stability limits and transformation pathways of α-quartz under high pressure. *Phys. Rev. B* **95**, 104112 (2017).

[32] Zhang, X.-J., Shang, C. & Liu, Z.-P. Pressure-induced silica quartz amorphization studied by iterative stochastic surface walking reaction sampling. *Phys. Chem. Chem. Phys.* **19**, 4725-4733 (2017).

[33] Pabst, W. & Gregorová, E. Elastic properties of silica polymorphs - A review. *Ceramics – Silikáty* **57**, 167-184 (2013).

[34] Brovchenko, I., Geiger, A. & Oleinikova, A. Liquid-liquid phase transitions in supercooled water studied by computer simulations of various water models. *J. Chem. Phys.* **123**, 044515 (2005)

[35] Yang, X., Tong, H., Wang, W.H. & Chen, K. Emergence and percolation of rigid domains during the colloidal glass transition. *Phys. Rev. E.* **99**, 062610 (2019).

[36] Ojovan, M.I. & Louzguine-Luzgin, D.V. Revealing structural changes at glass transition via radial distribution functions. *J. Phys. Chem. B* **124**, 3186-3194 (2020).

[37] Tong, H., Sengupta,S. & Tanaka, H. Emergent solidity of amorphous materials as a consequence of mechanical self-organisation. *Nat. Commun.* **11**, 4863 (2020).

[38] Bo Li, B., Lou, K., Kob, K. & Granick, S. Anatomy of cage formation in a two-dimensional glass-forming liquid. *Nature* **587**, 225 (2020).

[39] Carré, A., Berthier, L., Horbach, J., Ispas, S. & Kob, W. Amorphous silica modeled with truncated and screened Coulomb interactions: A molecular dynamics simulation study. *J. Chem. Phys.* **127**, 114512 (2007).

[40] Koehler, C., Hajnal, Z., Deak, P., Frauenheim, T. & Suhai, S. Theoretical investigation of carbon defects and diffusion in α-quartz. *Phys. Rev. B* **64**, 085333 (2001).

[41] Zwijnenburg, M.A., van Alsenoy, C. & Maschmeyer, T. Factors affecting ionicity in all-Silica materials: A Density Functional cluster study. *J. Phys. Chem. A* **106**, 12376–12385 (2002).

[42] Gibbs, G.V. *et al.* Bonded interactions in silica polymorphs, silicates, and siloxane molecules. *Amer. Mineral.* **94**, 1085–1102 (2009).

[43] Binder, K. & Kob, W. *Glassy materials and disordered solids* (Word Scientific, 2005).

[44] http://www.ncnr.nist.gov/resources/n-lengths/

[45] Fischer, H.E., Barnes, A.C. & Salmon, P.S. Neutron and X-ray diffraction studies of liquids and glasses. *Rep. Prog. Phys.* **69**, 233–299 (2006).

[46] Waasmaier, D. & Kirfel, A. New analytical scattering-factor functions for free atoms and ions for free atoms and ions. *Acta Crystallogr.* **A51**, 416–431 (1995).

[47] More1, S., Andrey, V., Kravtsov, A.V., Dalal, N. & Gottlöber, S. The overdensity and masses of the Friends-of-Friends halos and universality of halo mass function. *Astrophys. J Suppl. Ser.* **195**, 4 (2011).

[48] Zha, C.-S., Hemley, R.J., Maom, H.-k., Duffy, T.S. & Meade, C. Acoustic velocities and refractive index of SiO2 glass to 57.5 GPa by Brillouin scattering. *Phys. Rev. B* **50**, 13105 (1994).

[49] Petitgirard, S. *et al.* SiO_2 Glass density to lower-mantle pressures. *Phys. Rev. Lett.* **119**, 215701 (2017).

[50] Inorganic Crystal Structure Database. https://www.ccdc.cam.ac.uk/structures/

[51] Scheidl, K.S., Kurnosov, A., Boffa Ballaran, D.M., Angel R.J., & Miletich, R. Extending the single-crystal quartz pressure gauge up to hydrostatic pressure of 19 GPa, *J. Appl. Cryst.* **49**, 2129-2137 (2016).

[52] Buchen, J. *et al.* Equation of state of polycrystalline stishovite across the tetragonal-orthorhombic phase transition. *J. Geophys. Res. Solid Earth* **123**, 7347–7360 (2018).

[53] Hasmy, A., Foret, M., Pelous, J., & Jullien, R. Small-angle neutron-scattering investigation of short-range correlations in fractal aerogels: Simulations and experiments. *Phys. Rev. B* **48**, 9345-9353 (1993).

Acknowledgements: The authors would like to thank the BioNano-NMRI team (L2C, UM) for computer facilities. One of us (A.H) acknowledges support from the CNRS (France) and thanks L.C. Rincón for introducing him in the SCC-DFTB method. This work was done with the support of the Centre Informatique National de l'Enseignement Supérieur (CINES, France) via a Resource Allocation Panel award (project A0060910788).

Author contributions: All authors initiated the project. A.H. and B.H. performed the MD Tight-Binding (SCC-DFTB) calculations of the pressurized glasses, after S.I. has prepared the initial glass at ambient pressure by classical MD simulations. A.H. performed the tight binding calculations of the crystals and computed the percolation tools. All authors contributed to the data analysis: atomic structure (A.H, B.H., S.I.), electronic structure and percolation (A.H.), and inelastic structure factors (S.I.). A.H. and B.H. developed the main conclusions and wrote the paper, S.I. contributed to its final version.

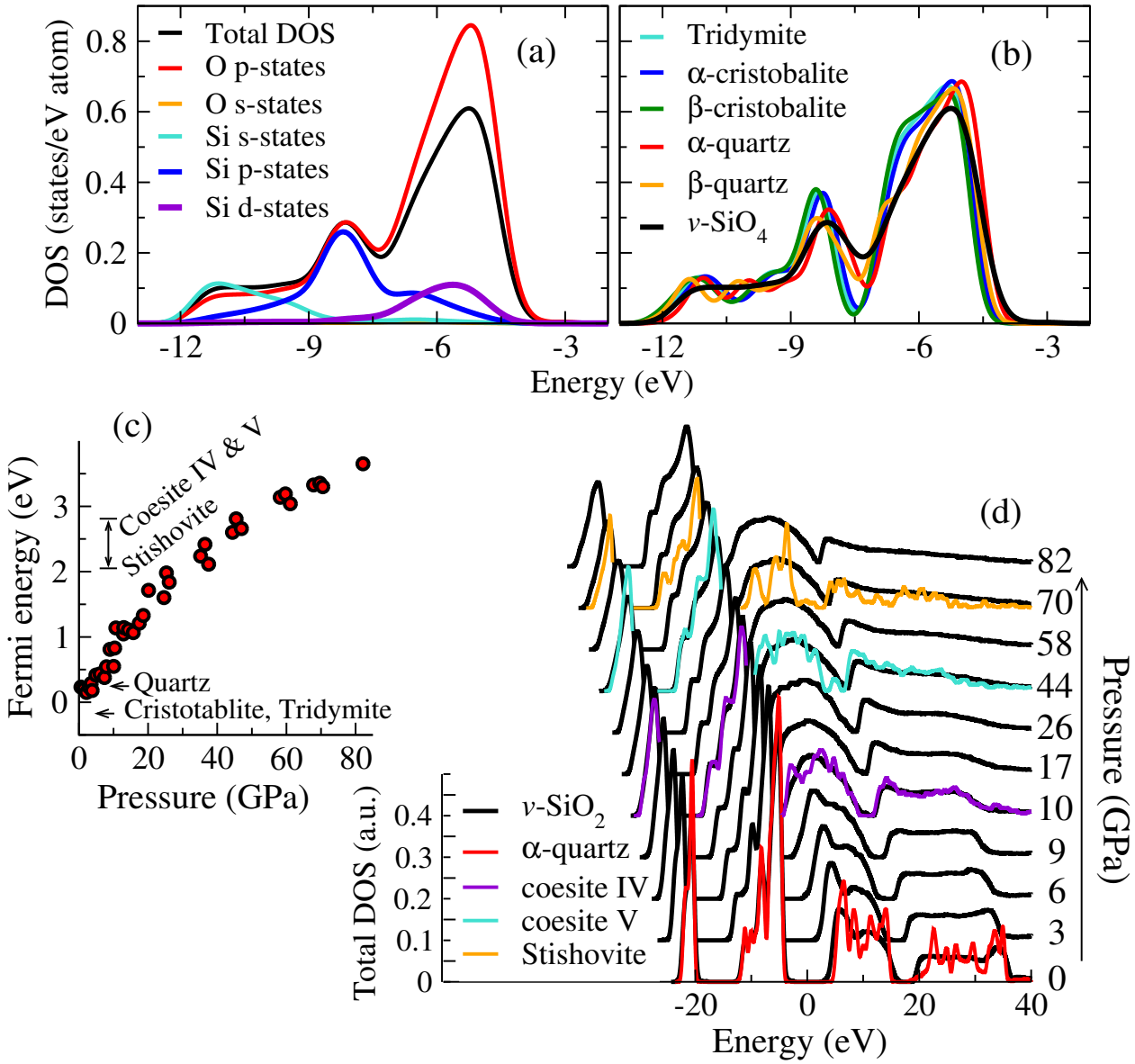

Extended Data Fig. 1. Total DOS for a SiO_2 glass at ambient pressure, with its corresponding projected DOS (a) and compared to different SiO_4 crystalline polymorphs (b). Fermi energy (c) and total DOS (d) when the pressure increases. The results are compared with those corresponding to different SiO_2 crystalline polymorphs.

c-SiO_2			v-SiO_2		
Polymorph	Pressure (GPa)	Density (g/cm^3)	Pressure (GPa)	Density (g/cm^3)	Polyamorph
α-Quartz [31, 51]	0-25	2.6-3.6	0-3	2.3-2.7	SiO_4
			8-10	3.3-3.5	SiO_4, SiO_5
			10-13	3.5-3.8	SiO_4, SiO_5, SiO_6
Coesite IV [6]	30-49	4.2-4.5	13-23	3.8-4.0	v-Coesite IV
Coesite V [6]	45-70	4.6-4.7	23-40	4.1-4.3	v-Coestite V
Stishovite [52]	10-73	4.3-4.9	40-82	4.4-4.9	v-Stishovite

Extended Data Table I: Correspondence between pressure and density in c-SiO_2 polymorphs and comparison with the polyamorph phases of v-SiO_2 defined in the text.

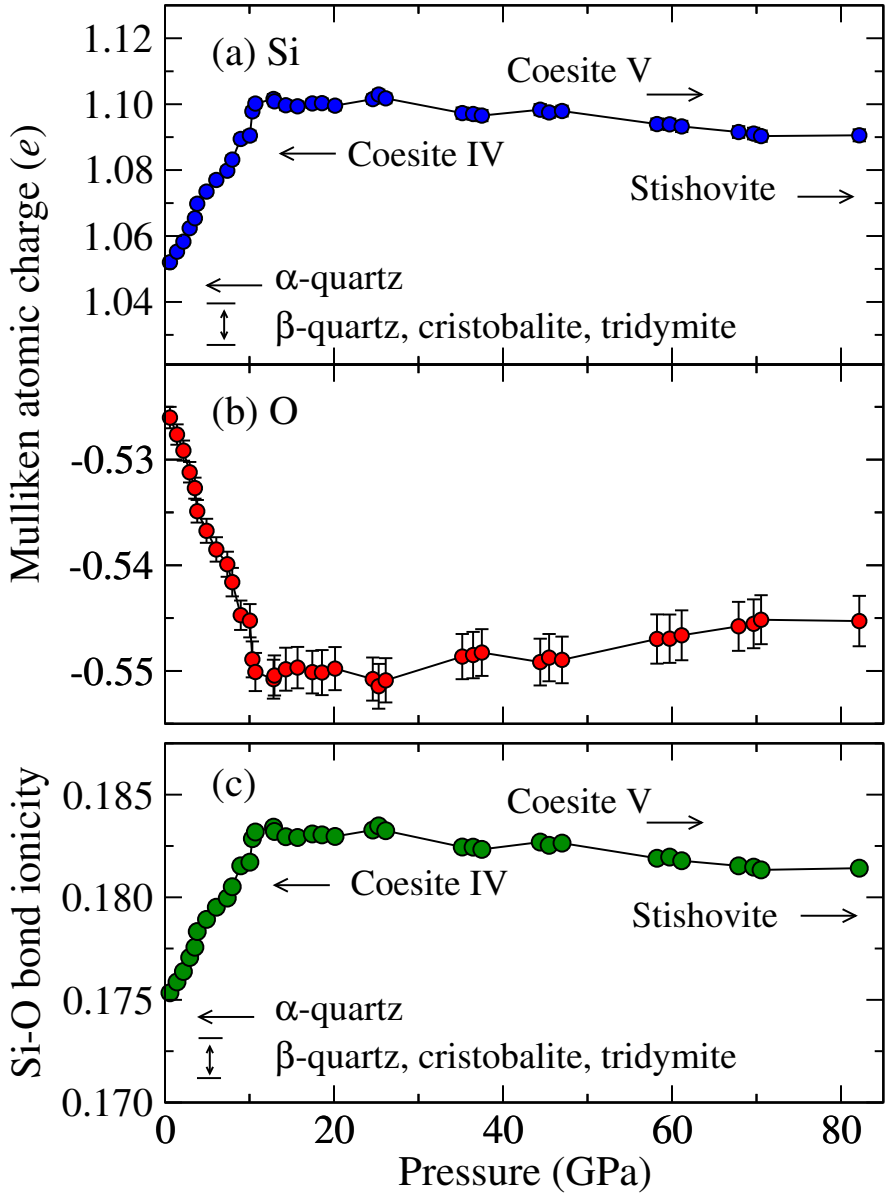

Extended Data Fig. 2. Mulliken atomic charges for Si (a) and O (b), and the average Mulliken ionicity of the Si-O bond (c) as a function of pressure. The results are compared with those corresponding to different SiO_2 crystalline polymorphs.

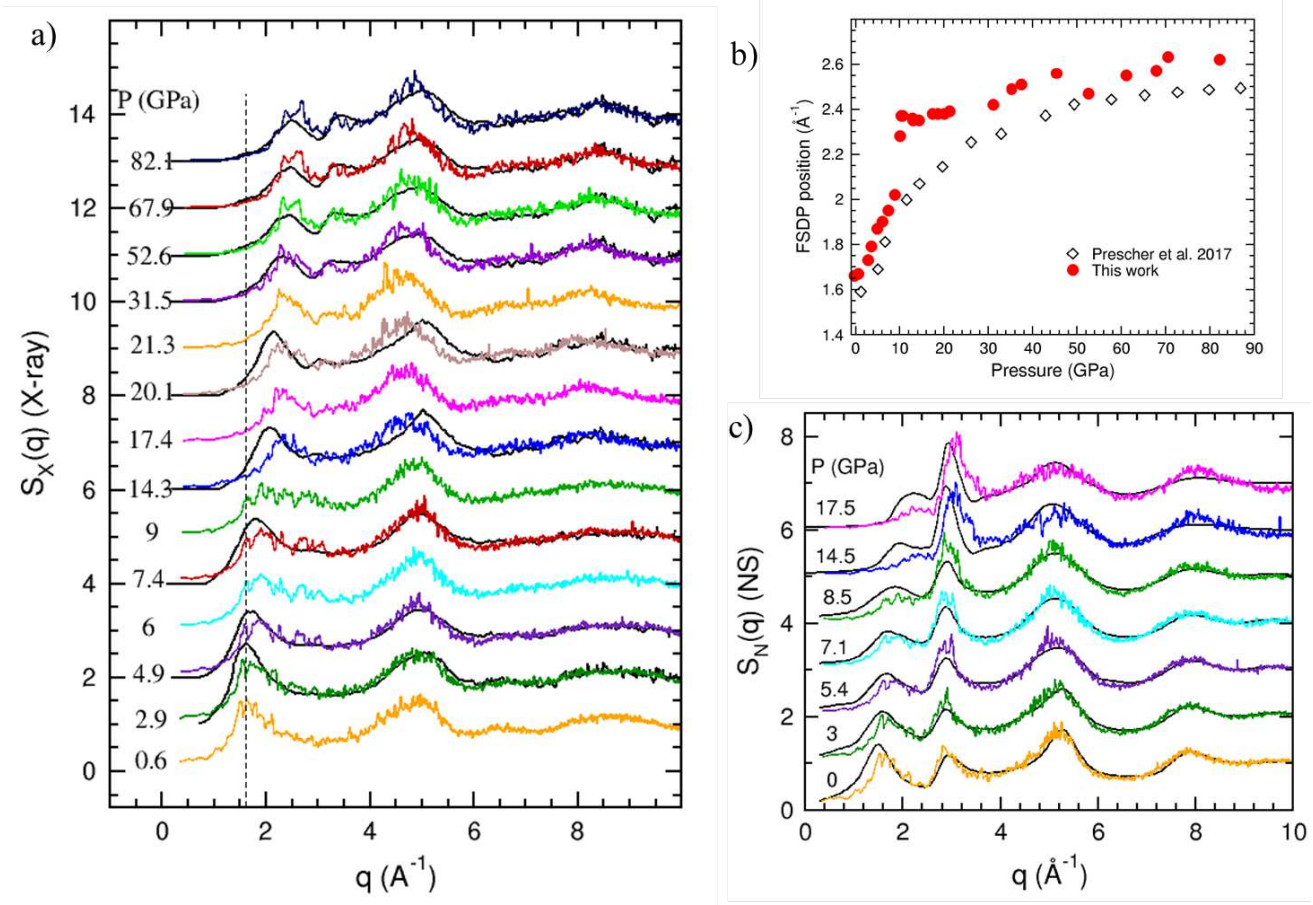

Extended Data Fig 3. $S_X(q)$ of our densified silicas compared to X-Ray data reproduced from Prescher *et al.* [3] and b) Evolution of the maximum of the first sharp diffraction peak FSDP. c) Calculated $S_N(q)$ compared to neutron data (black lines) reproduced from Zeidler *et al.* [13].

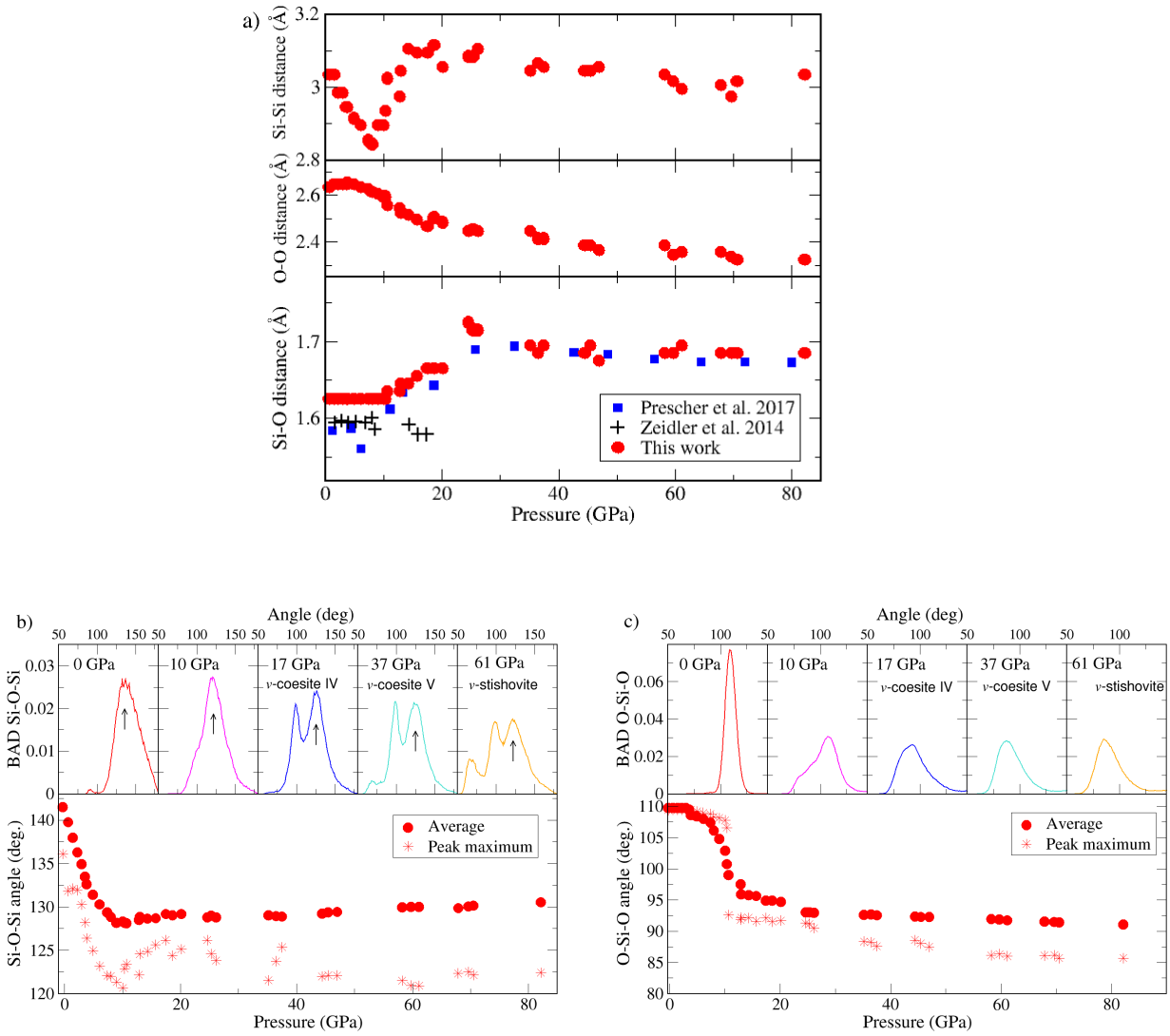

Extended Data Fig. 4: (a) Calculated Si-O, O-O, and Si-Si bond length at maximum of the distribution. Si-O distances are compared to X-Ray (squares) and neutron (+) scattering data. (b) Si-O-Si bond angle distribution (BAD) and pressure dependence of the Si-O-Si BAD marked by the arrow. The average value has been calculated from 110° to 175°. (c) Pressure dependence of the O-Si-O and examples of bond angle distributions (BAD).

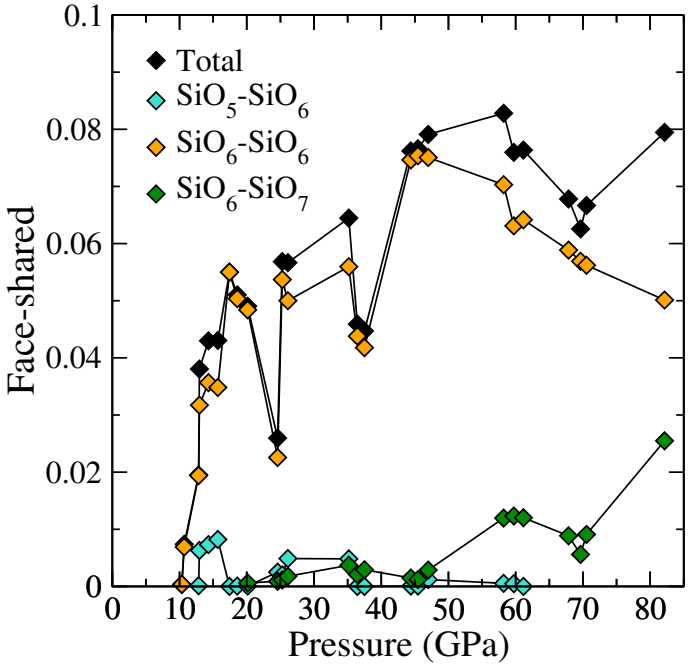

Extended Data Fig 5. Number of face-sharing per polyhedron unit for dominant SiO_n-SiO_m connectivities as a function of pressure.

Figures

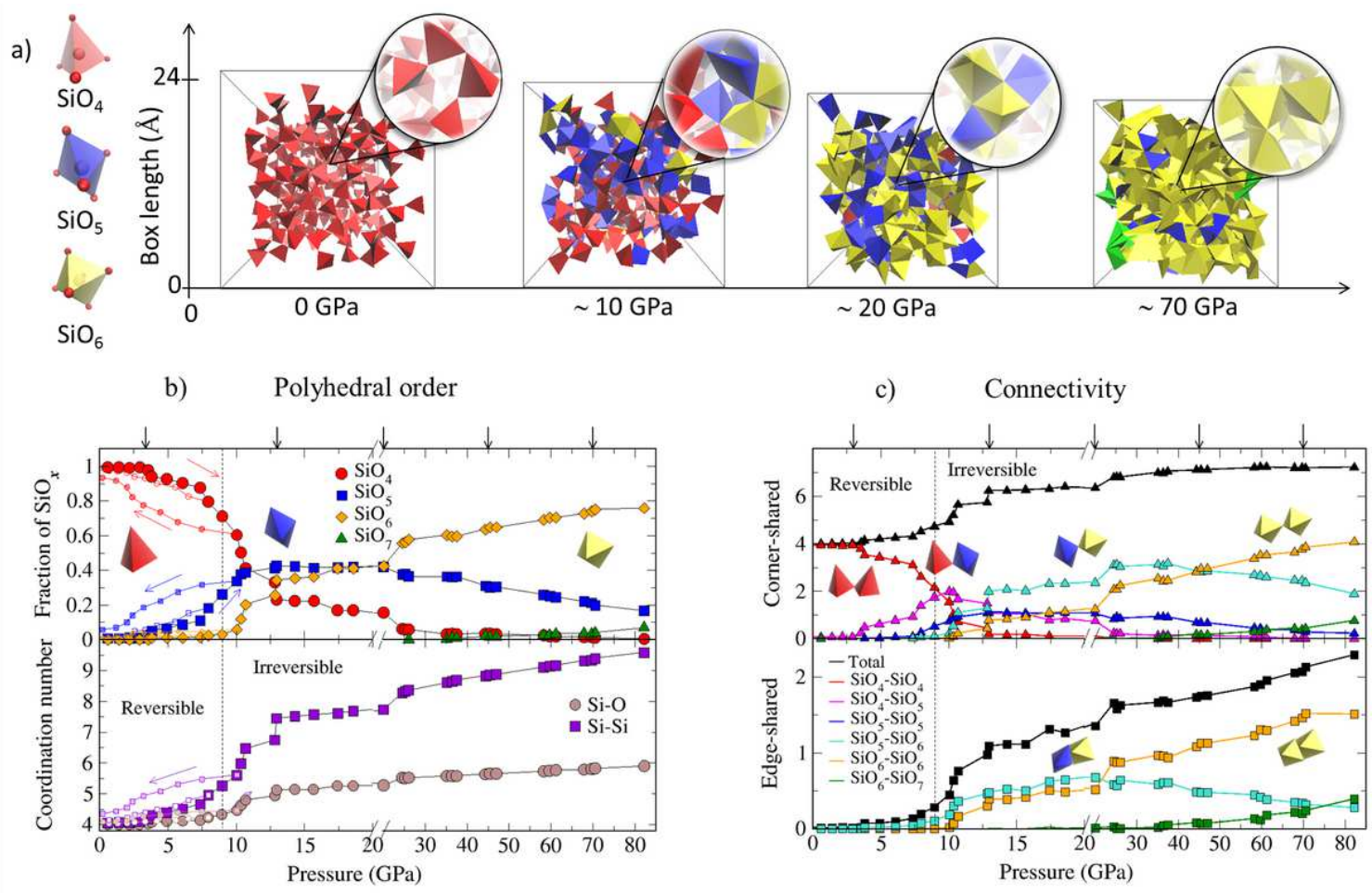

Figure 1

(a) Snapshots of the simulation boxes showing the evolution of the short range structures from SiOn to SiOn+1 polyhedra, and of their connectivity from corner- to edge-sharing connectivity (circular insets), upon pressure. The glass samples are pressurized by instantaneous reduction of the simulation box followed by a relaxation using periodic boundary conditions. (b) Fraction of Si polyhedra and Si-O and Si-Si coordination number as a function of pressure. Small symbols and arrows nearby correspond to unloadings from 8 GPa and slightly above 10 GPa. (c) Shared corners and shared edges per polyhedron. The bold vertical arrows on top in panels (b,c) mark the onset of the different regimes (see text) and the dashed line indicates the elastic to plastic transition. Note that the scale changes at 20 GPa in the abscissa axis.

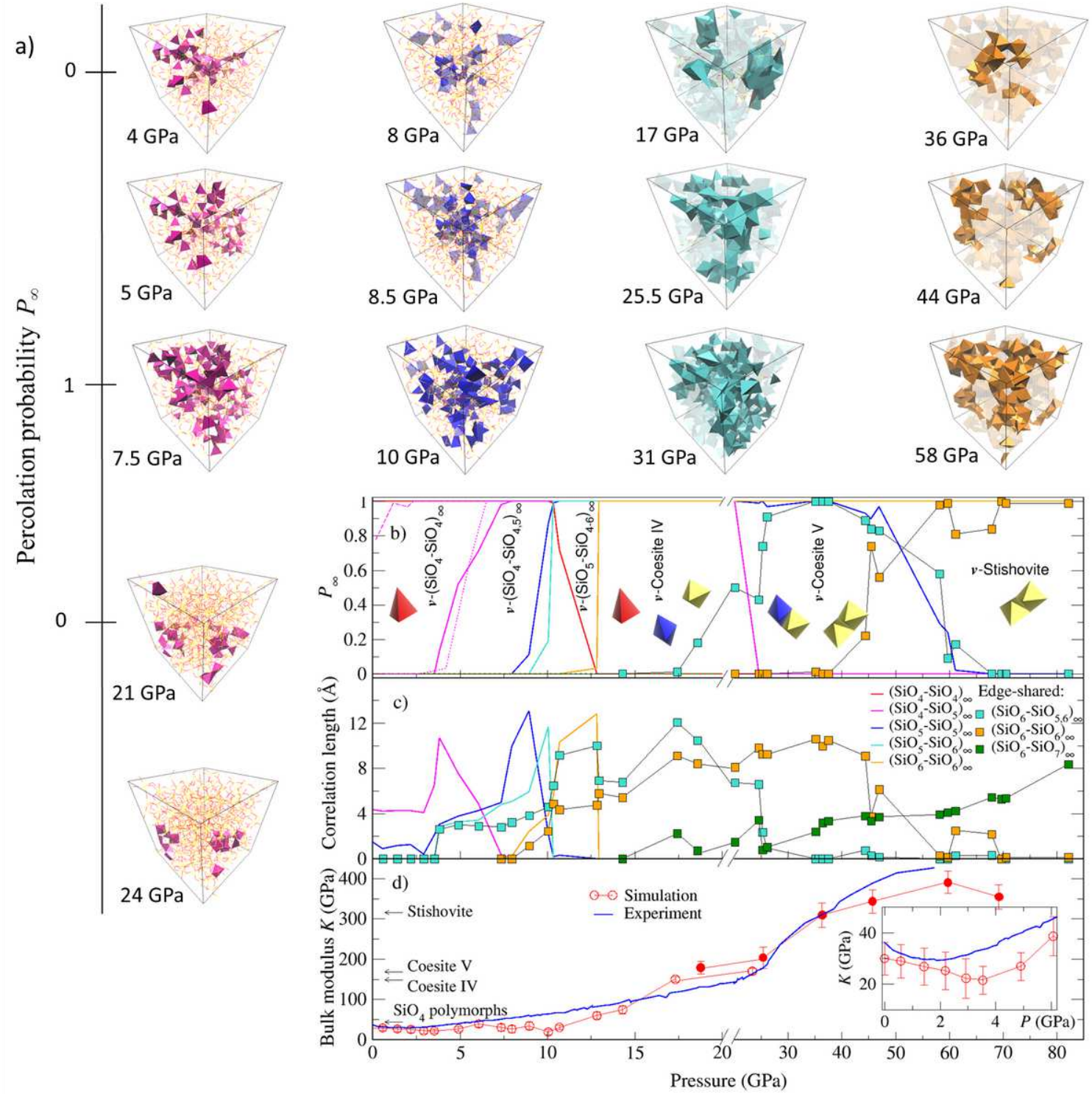

Figure 2

(a) Snapshot of the spanning clusters in the simulation box for pressures corresponding to P1 = 0 up-to P1 = 1, and back to P1 = 0 for the first one. From left to right: corner-shared (SiO4-SiO5)1 and (SiO5-SiO5)1 clusters, and edge-shared (SiO6-SiO5;6)1 and (SiO6-SiO6)1 clusters. (b) Percolation probability, P1, versus pressure for the different 4-, 5-, 6- and 7- folded coordinated Si, and their combinations. Dashed and dotted magenta lines correspond to P1 of the cluster (SiO4-SiO5)1 for decompression from 8 GPa and 10 GPa, respectively. (c) Correlation length of the percolating clusters in panel (b). (d) Bulk modulus K

as function of pressure, and comparison with high frequency experiments (unrelaxed bulk modulus) [16]. The inset zooms on the low pressure region. Note that the scale changes at 20 GPa in the abscissa axis.

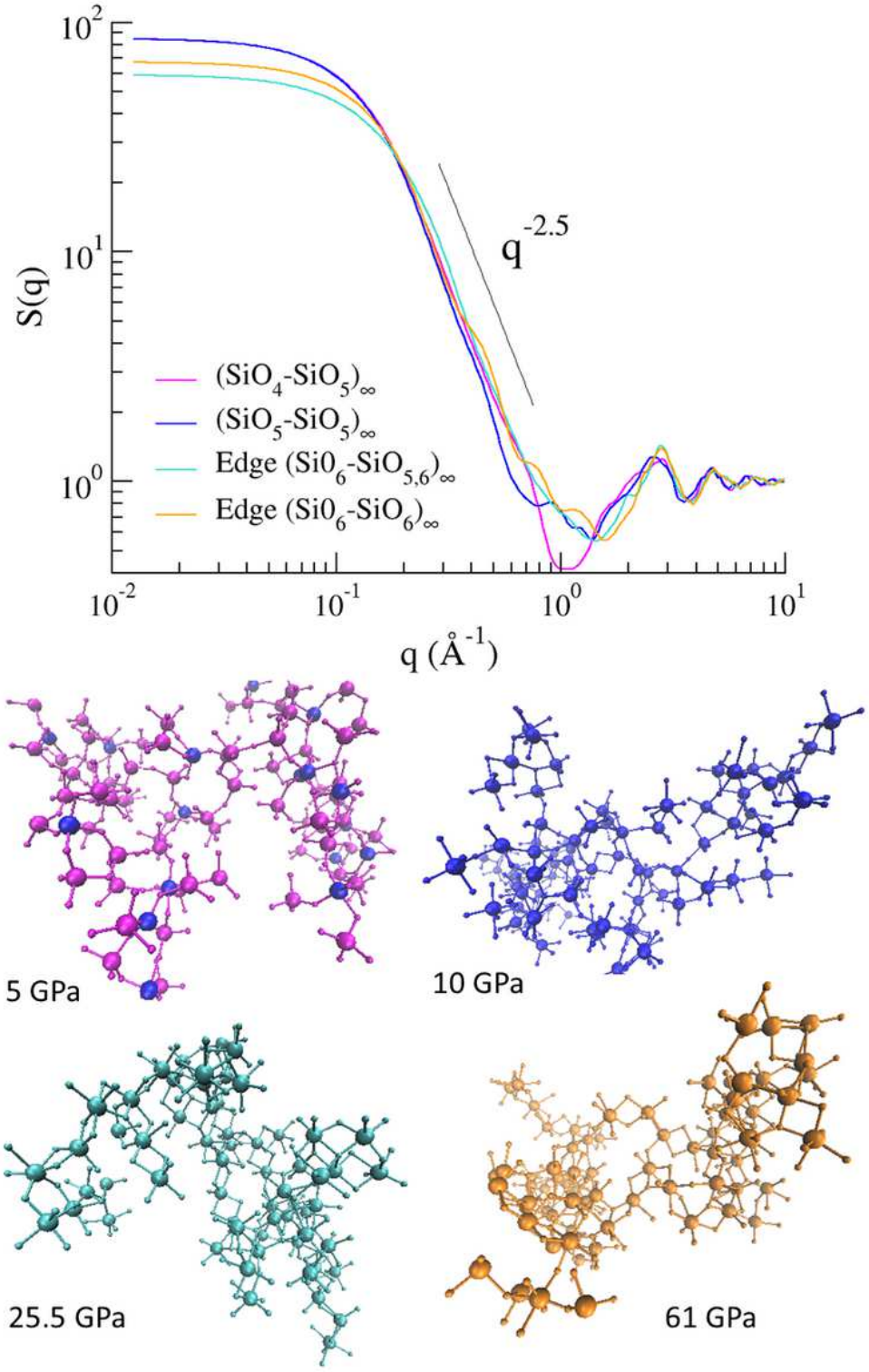

Figure 3

Structure factors S(q) for the isolated and extended percolating clusters at the critical pressures (indicated in the snapshots) in log-log scale.